Lola Mugisho ORCID iD: 0000-0002-4519-6727

The influence of hyperglycaemia on the safety of ultrasound in retinal pigment epithelial cells

Authors:

Heather Kang[1], Naibo Yin[1, 2], Heather Lyon[1], Ilva D Rupenthal[1], Sachin S Thakur[1, 2], Odunayo O Mugisho[1]

Affiliations:

[1]Buchanan Ocular Therapeutics Unit, Department of Ophthalmology, New Zealand National Eye Centre, Faculty of Medical and Health Sciences, University of Auckland, Auckland, New Zealand

[2]School of Pharmacy, Faculty of Medical and Health Sciences, University of Auckland, Auckland, New Zealand

Short running title:

Hyperglycaemia modulates ultrasound effects

Corresponding Authors:

1. Odunayo O Mugisho

Tel.: +64 9 923 8274

Email address: lola.mugisho@auckland.ac.nz

ORCID iD: 0000-0002-4519-6727

2. Sachin S Thakur

This article has been accepted for publication and undergone full peer review but has not been through the copyediting, typesetting, pagination and proofreading process, which may lead to differences between this version and the Version of Record. Please cite this article as doi: 10.1002/cbin.11477.

Tel: +64 9 923 7199

Email address: s.thakur@auckland.ac.nz

ORCID iD: 0000-0003-4910-0005

Keywords: Ultrasound; Diabetic retinopathy; Hyperglycaemia; Retinal pigment epithelium

Abbreviations:

DR Diabetic retinopathy

LDH Lactate dehydrogenase

NF-κB Nuclear factor-kappaB

RPE Retinal pigment epithelium

US Ultrasound

VEGF Vascular endothelial growth factor

ZO-1 Zonula occluden-1

Abstract

Ultrasound (US) assisted drug delivery is receiving interest in treating posterior eye diseases such as diabetic retinopathy (DR) due to its ability to maximise drug penetration into difficult to reach tissues. Despite its promise, the technique has only been investigated using healthy cell and tissue models, with no evidence to date about its safety in active disease. As a result, the aim of this study was to evaluate the safety of US administration *in vitro* in retinal pigment epithelial cells under normal and high glucose conditions. US protocols within the presently accepted safety threshold were applied and their influence on cell membrane and tight junction integrity as well as intracellular inflammation was evaluated using lactate dehydrogenase (LDH), zona occludens-1 (ZO-1), FITC-dextran dye leak and NF-κB assays, respectively. Under high glucose conditions, US application increased LDH release and resulted in loss of ZO-1 labelling at 2 h; however, normal levels were restored within 24 h. US within its

safety parameters did not induce any FITC-dextran dye leak or NF-κB nuclear translocation in normal or high glucose conditions. In conclusion, our results suggest that while high glucose conditions increase cell susceptibility to US-mediated stress, basal conditions can be restored within 24 h without long-lasting cell damage.

1. Introduction

Diabetic retinopathy (DR) is a chronic inflammatory condition that affects the retina and can lead to vision loss. DR, in its late stages, is associated with severe vascular pathology characterised by the presence of microaneurysms, haemorrhages, and neovascularisation (Nentwich and Ulbig 2015). Currently, the gold-standard to treat DR includes anti-vascular endothelial growth factors (anti-VEGF) although their long-term use has been linked to the development of geographic atrophy (Martin, Maguire et al. 2012, Gemenetzi, Lotery et al. 2017), a decrease in choroidal thickness (Grunwald, Daniel et al. 2014), and loss of retinal ganglion cells (Nishijima, Ng et al. 2007). Furthermore, anti-VEGF therapy requires repeated intravitreal injections, which are a painful and inconvenient method of treatment associated with risks of infections and accidental retinal detachment.

Despite the limitations associated with intravitreal anti-VEGF therapy, alternative treatment avenues are not forthcoming because of the notable difficulty in reaching the cells implicated in posterior eye diseases such as DR (Thrimawithana, Young et al. 2011). This is because DR affects cells in the retina, which is located on the inside at the back of the eye and is protected by many anatomical and physiological barriers. Treatment using an eyedrop would require the drug to first withstand being washed away by the tear fluid and next permeate through the collagenous corneal or scleral external layers of the eye before migrating through various intraocular tissues or choroidal blood vessels to finally reach the retina (Geroski and Edelhauser 2000, Hughes, Olejnik et al. 2005). In the case of a systemic administration, drug in the bloodstream would need to traverse the poorly permeable blood-retinal barrier, which features a collection of endothelial and epithelial cells along with pericytes and glial cells packed in close association (Cunha-Vaz 2013). In both cases, only a fraction of the administered dose can reach the target site, with both high wastage and a prevalence of off target side effects observed. Recent studies have suggested that the current difficulties faced in treating posterior eye disease may be addressed using

ultrasound (US) (Huang, Chen et al. 2017, Thakur, Ward et al. 2017, Thakur, Chen et al. 2019). This technique has been widely explored given its routine use on the human body. When used in the realm of drug delivery, the technique has demonstrated an ability to improve molecular permeation through many tissues within the body (Pereira, Ramos et al. 2017, Thakur, Ward et al. 2017, Zhang, Yan et al. 2018, Wei, Shang et al. 2019). In the context of posterior eye disease, US has demonstrated an ability to improve molecular permeation through the sclera (Shah and Zderic 2009, Suen, Wong et al. 2013, Lafond, Aptel et al. 2017), vitreous humour (Sonoda, Tachibana et al. 2012, Thakur, Chen et al. 2019), and blood-retinal barrier (Park, Zhang et al. 2012) as well as into specific cells of the retina (Huang, Chen et al. 2017, Thakur, Ward et al. 2017).

US improves drug delivery into tissues via acoustic cavitation. Here, the applied stimulus induces the formation and growth of tiny gas cavitation nuclei within body fluids (Domenici, Giliberti et al. 2014). US causes the gas nuclei to oscillate, which results in stable and inertial cavitation. The periodic oscillation of stably cavitating gas bubbles may produce microstreams, which are shear forces exerted by the fluid circulation onto the plasma membranes of nearby cells (Lentacker, De Cock et al. 2014). Conversely, the rapid growth and subsequent collapse of inertial cavitating bubbles produces an instantaneous release of a high volume of energy (Paliwal and Mitragotri 2006). This occurs in the form of a microjet, which may perforate nearby cells. Both microstreaming and microjets exert mechanical stresses onto the membrane of cells which result in temporary minute wound-like pores in the plasma membrane. This phenomenon is known as sonoporation (Paliwal and Mitragotri 2006, De Cock, Zagato et al. 2015), which is thought to reversibly and transiently enhance drug molecule permeation, after which the wound-like pores are repaired through endogenous mechanisms. This is essential to maintain cell integrity and normal physiological function (Schlicher, Radhakrishna et al. 2006).

Several studies have suggested different ways in which US-mediated drug delivery can increase drug uptake into the retina when combined with clinically relevant administration strategies. It has been shown that intravitreal, trans-scleral or suprachoroidal injection of a depot formulation could be followed by trans-scleral US application to induce drug release as and when required (Kim, Prausnitz et al. 2013,

Huang, Chen et al. 2017, Agban, Thakur et al. 2019, Thakur, Chen et al. 2019). In another instance, US following intravitreal injection was used to encourage particle movement into the retina while also enhancing cell permeability (Thakur, Chen et al. 2019). Despite the benefits associated with the use of US for retinal drug delivery, its use in susceptible unhealthy tissue carries additional risks of causing mechanical, chemical and thermal stress to the tissue (Phenix, Togtema et al. 2014). Additionally, previous studies have assessed US safety under normal conditions despite the fact that, in reality, US would likely be applied to enhance drug delivery in disease where the safety threshold may be different (Peeters, Lentacker et al. 2008, Xie, Liu et al. 2010, Park, Zhang et al. 2012, Thakur, Ward et al. 2017). This is particularly important in chronic diseases where repeated treatments are often required over several years. It is therefore imperative to assess US safety in both healthy and diseased conditions to establish whether the nature of a disease may increase susceptibility to US-related injury. In light of this, we evaluated the safety of US administration in retinal pigment epithelial (RPE) cells under normal and hyperglycaemic conditions. Hyperglycaemia is a key pathology in DR and we previously observed *in vitro* and *in vivo* that hyperglycaemia increases the cells' susceptibility to inflammatory cytokine-mediated injury (Mugisho, Green et al. 2018, Mugisho, Green et al. 2018, Kuo, Green et al. 2020). Other studies have also reported that high glucose can induce oxidative stress during RPE migration which could make the cells more susceptible to other forms of injury (Farnoodian, Halbach et al. 2016).

In the first instance, we identified a series of US protocols that cause differing levels of temperature elevations in RPE cells. Secondly, changes in cell membrane permeability were assessed using a lactate dehydrogenase (LDH) assay. To assess the integrity of an RPE monolayer following US application, zonula occludens-1 (ZO-1; tight junction marker) and FITC-dextran dye leak were measured under normal and high glucose conditions. Finally, we determined US induced inflammation in the cells by labelling for nuclear factor-kappa B (NF-κB) using immunohistochemistry.

2. Materials and methods

2.1.Materials

Human adult retinal pigment epithelial cells (ARPE-19) were purchased from the American Type Culture Collection (ATCC, Manassas, VA, USA). Dulbecco's

Modified Eagle Medium Nutrient Mixture F-12 (DMEM-F12) and 100x antibiotic-antimycotic (AA) were purchased from Thermofisher Scientific Inc. (Waltham, MA, USA). Foetal bovine serum (FBS) as well as rabbit anti-ZO-1 and goat anti-rabbit Alexa488 antibodies were purchased from Invitrogen (Carlsbad, CA, USA). LDH detection kit was purchased from Roche Diagnostics (Auckland, NZ). Rabbit anti-NF-κB antibody was purchased from Abcam (Cambridge, UK). Cell nuclei stain, DAPI, was purchased from Sigma-Aldrich (St Louis, MO, USA).

2.2.Cell culture

ARPE-19 cells were cultured in growth medium containing DMEM-F12 supplemented with 10% FBS, and 1x AA. Cells were grown in T75 flasks and incubated at 37 °C in a humidified 5% CO_2 incubator until confluent. Cells were used between passage 6 and 12. For experiments, cells were seeded at a density of 2.5 x 10^5 cells/well in 24 well plates without (for LDH assays) or with coverslips (for immunohistochemistry).

2.3.Thermal study

Infrared thermography was used to evaluate culture medium temperature changes following US exposure. US of 1 MHz was applied to the bottom of the culture plates for 1 min using a SONOPLUS 190 US machine equipped with a 10 mm diameter probe (Enraf-Nonius, Rotterdam, Netherlands). US intensity and duty cycle (DC) were varied from 0-1 W/cm^2 and 0-100%, respectively. A thermographic camera TVS-200EX (NEC Avio Infrared Technologies co., San Fernando, CA, USA) was used to take heat zone images and record the medium temperature before and after US application.

2.4.High glucose treatment

High glucose conditions were induced as previously described (Mugisho, Rupenthal et al. 2018). Briefly, cells were first placed in media containing normal glucose for 48 h until confluence was achieved. Cell culture media were then changed to either normal (17.5 mM) or high glucose (37.5 mM) conditions for 24 h.

2.5.US administration

Administration of US was carried out in alternating wells of a 24 well plate to prevent overlap (Fig. 1). Four US doses of varying intensity and DC were selected based on the findings of the thermal study. These were basal (no US), low US (0.2 W/cm^2 and 50% DC), high US (0.5 W/cm^2 and 50% DC), and positive control (PC; 1.0 W/cm^2 and 100% DC). Each US treatment was applied for 1 min. The four US doses were tested in both normal and hyperglycaemic conditions.

2.6.Assessment of LDH release

An LDH assay was used as previously described (Mugisho, Rupenthal et al. 2018) to assess the degree of mechanical stress that US may place on cells. LDH may be released by cells via pores induced by sonoporation or other openings due to cellular injury. Briefly, following US administration, samples were re-incubated and 50 µl aliquots of the medium were withdrawn 30 min and 2 h after, respectively. The amount of LDH released into the cell culture medium was measured using an LDH assay kit according to manufacturer instructions. Absorbance was measured at 490 nm using a SpectraMax i3x spectrophotometer (Molecular Devices, San Jose, CA, USA).

2.7.Metabolic activity using an MTT assay

Metabolic activity was measured using an MTT assay. ARPE-19 cells were seeded onto 24-well plates at a density of 2×10^5 cells/mL. Cells were incubated with high or normal glucose for 24 h before US application. After 2 h, spent media was removed and 200 µL of MTT solution (5 mg/mL) was added to each well and incubated at 37 °C for 4 h. The MTT solution was then removed and replaced with 100 µL of 0.04 M HCl in absolute isopropanol. The absorbance was measured using a SpectraMax i3x spectrophotometer (Molecular Devices, San Jose, CA, USA) at a wavelength of 570 nm with background subtraction at 650 nm.

2.8.Measurement of FITC-dextran paracellular permeability

Cells were seeded at $2.5x10^5$ cells/mL on polyester membranes in Transwell® 24-well plates (Corning Incorporated, Corning, NY, USA) in growth medium and incubated for 24 h in normal or high glucose media. Inserts were removed and placed gently into

a 6-well plate without media to optimise contact between the US probe and the cell layer. US treatment was then conducted on the inserts in the 6 well plate as previously described. Once the inserts were returned to their respective treatment media, cellular barrier integrity was measured by assessing the movement of 70 kDa fluorescein isothiocyanate (FITC)-dextran (D1820, Thermofisher Scientific Inc., Waltham, MA, USA) across a monolayer of cells as previously described. Briefly, 100 µL of FITC-dextran (10 µg/mL) was added to the inserts and incubated for 15 min. Inserts were then removed and samples transferred to 96-well plates for quantification by spectrophotometry (excitation 490 nm and emission 520 nm). FITC-dextran permeability was expressed as a percentage relative to basal conditions. The sample size was three readings per well for each treatment then the entire experiment was repeated three times.

2.9.Immunohistochemistry

Cells were seeded in 24-well plates containing coverslips for immunohistochemistry. Following treatments, cells were fixed with 4% paraformaldehyde for 10 min and permeabilised with 0.1% Triton X-100 in phosphate buffer saline (PBS) for 10 min. Cells were then incubated with either rabbit anti-ZO-1 (1:500) or rabbit anti-NF-κB (1:500) at 4 °C overnight followed by washing in PBS three times for 15 min. Goat anti-rabbit Alexa-488 (1:500) secondary antibody was applied and incubated at room temperature for 3 h. Secondary-only controls revealed no non-specific labelling. Cell nuclei were stained with DAPI (1:1000) and slides were mounted using Citifluor™ anti-fade reagent. ZO-1 expression was assessed at 2 and 24 h while NF-κB was only assessed at 24 h. Labelling was repeated three times in separate experiments.

2.10. Statistical analysis

Data are presented as arithmetic means + S.E.M. Statistical comparisons between groups were performed using one-way or two-way ANOVA with Dunnett's multiple corrections test using GraphPad Prism 6 (San Diego, CA, USA). The specific statistical method used for each data set is provided in the respective figure legend. Adjusted $p < 0.05$ was considered to indicate statistically significant differences.

3. Results

3.1. An increase in US intensity correlates with an increase in medium temperature

In order to determine the effect of US on the medium temperature, we looked at the effect of both US power (W/cm^2) and DC (%). DC corresponds to the percentage of the time during which ultrasound is on during it application; therefore, a DC of 50% means that over a 100 ms application time, the US is on for 50 ms and off for 50 ms. As can be seen in Fig. 2, an increase in US intensity resulted in an increase in medium temperature. At the lowest US dose used (0.2 W/cm^2 + 20% DC), there was no statistically significant change in temperature relative to basal conditions. However, increasing the US intensity to 0.5 W/cm^2 or the DC to 50% led to a significant increase in temperature ($p < 0.05$). In spite of this, all test US conditions only increased the medium temperature by 0.5 to 1.0 °C. Conversely, the US dosage used for the PC (1.0 W/cm^2 + 100% DC) caused an increase in temperature which exceeded the recommended safety maximum of higher than 1.5 °C. Based on these thermal research outputs, the PC US dose was maintained to represent the effect of a detrimental US dose while the low and high US dosages of 0.2 W/cm^2 + 50% DC and 0.5 W/cm^2 + 50% DC, respectively, were chosen to be below this threshold.

3.2. High glucose conditions intensifies US-mediated LDH release

All subsequent evaluations were performed in both normal and high glucose conditions. In normal conditions, US application did not significantly change LDH release from ARPE-19 cells (Fig. 3a). An increase in LDH was observed 30 min following administration of the PC ($p< 0.05$), however this returned to baseline levels by 2 h. In the high glucose group, no changes in LDH release were seen 30 min following application of either the low or high treatment protocols. However, 2 h after administration, there was a dose-dependent increase in LDH release with the high US treatment group being significantly greater than baseline (Fig. 3b, $p< 0.01$). PC settings resulted in significantly greater LDH release than baseline at both timepoints under high glucose conditions.

3.3. US does not affect metabolic activity in normal or high glucose conditions

To determine whether changes in LDH release were due to cell death or transient transcellular permeability, cell images were analysed, and metabolic activity was measured using the MTT assay (Fig. 4). Cell images showed no changes in cell morphology across all treatment groups. While there were no significant changes in metabolic activity in normal glucose conditions, results showed that high glucose levels led to significantly increased metabolic activity following high US and PC treatments.

3.4. High glucose conditions worsens US-mediated loss of ZO-1 localisation at the cell membrane at 2 h

Given that the most significant changes in LDH release were observed at 2 h, the effect of high glucose and US treatment on tight junction protein expression and localisation was also studied at this timepoint. In both normal and high glucose conditions, ZO-1 was localised to the cell membrane (red arrows; Fig. 5a) without US application. On the contrary, there was a complete loss of ZO-1 at the tight junctions in PC groups under both glucose conditions. In the normal glucose group, some ZO-1 was still localised at the cell membrane with the low and high US dose, however this localisation was greatly reduced compared to basal levels. In the high glucose group, there appeared to be an increasing loss of ZO-1 localisation at the cell membrane with increasing US dose. Overall, the loss of ZO-1 localisation at the cell membrane observed in the high glucose group was more pronounced compared to the normal glucose group.

3.5. ZO-1 protein is restored to the cell membrane in both normal and high glucose conditions by 24 h

To determine the longevity of US-mediated changes to tight junctions, ZO-1 expression was evaluated again at 24 h. Results showed that by 24 h, there was a recovery of cell membrane-localised ZO-1 protein expression in both normal and high glucose groups and for both low and high US doses (Fig. 5b). However, the PC groups for both glucose conditions did not show recovery of ZO-1 localisation.

3.6. US treatment induces prolonged changes in paracellular dye permeability only in the PC group in high glucose conditions

In order to determine whether the changes to ZO-1 expression translated into loss of barrier integrity, the permeability of a monolayer of ARPE-19 cells was assessed using FITC-dextran (Fig. 6). At 2 h, results showed that only the PC groups induced FITC-dextran dye leak across the monolayer in both normal and high glucose conditions. By 24 h, FITC-dextran dye leak persisted in the PC treated group for the high glucose condition only while barrier integrity was recovered in all other cases.

3.7. US treatment does not induce nuclear translocation of NF-κB under high glucose conditions

To evaluate the effect of glucose levels and US treatment on cellular inflammation, translocation of NF-κB from the cell membrane into the nucleus was examined (Fig. 7). Results showed that there was no NF-κB translocation into the cell nucleus at both 2 h (results not shown) and 24 h (Fig. 7) in all groups studied.

4. Discussion

The primary objective of this study was to evaluate whether US was equally safe when administered to cells in normal and high glucose conditions. Earlier studies on the use of clinical US have identified 1.5 °C as the maximum temperature increase allowable for the technique to be considered as ‘safe’ for application to the eye (Nabili, Geist et al. 2015). As a result, we first set out to identify how different ultrasonic parameters influence post-administration temperature. Due to the fact that higher baseline temperatures result in lower resolution, experiments were conducted at room temperature. As a result, media without cells were used because normalising cells to room temperature was likely to induce cell stress itself negatively impacting the results. The highest US parameter was set to 1.0 W/cm^2 and 100% DC (positive control; PC) based on observations made using our apparatus in previous studies on ocular tissues (Huang, Chen et al. 2017). A range of US parameters were chosen lower than the PC by varying both the intensity and DC. Unsurprisingly, it was revealed that both increasing intensity and DC increased the medium temperature, with PC increasing the temperature above the recommended safety maximum of 1.5

°C. Interestingly, 20% DC resulted in higher temperature variability compared to 50% DC suggesting that the output from lower DC was less predictable. As a result, we elected to progress with two safe protocols with increasing intensity while keeping the DC constant at 50%.

While the thermal stress caused by US may be a useful measure to indicate its ocular safety, it does not allude to molecular changes that might occur due to mechanical and chemical stresses created by this technique. As a result, to understand the various mechanisms by which US may cause cellular stress, we assessed the cellular responses to the stimuli through a variety of assays. The LDH assay was used to evaluate the leakiness of the cellular membrane. It is well established that US increases cell permeability, but it is also important to ensure that this occurs in a transient manner (Schlicher, Radhakrishna et al. 2006, Thakur, Ward et al. 2017). At 30 min, only the PC settings induced significant LDH release in the normal glucose state and this was restored to basal levels by 2 h indicating that US-mediated cellular leakage was transient with no long-term impact on cellular wellbeing. Interestingly, in high glucose conditions, a significant and prolonged increase in permeability was observed in both the high US (0.5 W/cm^2 and 50% DC) and PC groups, providing the first evidence that the cellular response to the US stimulus may differ based on the glycaemic state. These results were not entirely surprising given that previous studies have reported that hyperglycaemia increases cellular susceptibility to stress and inflammation (Calado, Alves et al. 2016, Mugisho, Green et al. 2018). Nonetheless, given that the purpose of US application is therapeutic in nature, it is important to ensure that its negative effects in high glucose conditions is only temporary to support its role in enhancing cellular drug uptake without causing any damage. As a result, the next experiment evaluated cell morphology and metabolic activity at 2 h, the timepoint at which US appeared to mediate the most significant changes in LDH release. Interestingly, the results suggested that despite having a pronounced effect on LDH release, US treatment did not change cell morphology or reduce metabolic activity in both normal and high glucose conditions. Taken together, these findings suggest that US increases transcellular permeability without inducing cell death in both normal and high glucose conditions.

Having assessed transcellular permeability, the study evaluated paracellular permeability first by assessing the effect of US on the tight junction protein ZO-1 in ARPE-19 cells. This is of significance because RPE cells form the outer blood-retinal barrier that separates the choroid from the photoreceptors in the retina, a role that is crucial in the maintenance of retinal homeostasis (Xu, Song et al. 2011). Furthermore, for US-mediated drug delivery across this barrier, transient weakening of tight junctions may be advantageous to enable drug passage to the retina. Previous use of US to increase blood-brain barrier permeability showed that the stimulus disassembled the molecular structure of tight junctions at the cell junction and caused an overall decrease in the expression of tight junction proteins such as occludin, claudin-5 and ZO-1(Sheikov, McDannold et al. 2008).However, the study reported that the changes in tight junction proteins were restored back to basal levels after 4 h.

At 2 h, ZO-1 localization at the cell membrane was significantly reduced in all applied protocols indicating an increase in outer blood-retinal barrier permeability. While delocalization was greater in the hyperglycaemic group after 2 h, normal ZO-1 localization was restored by 24 h in both glycaemic conditions for the low and high US groups, showing that the tight junctions were able to recover in both instances. In addition to ZO-1 localisation, FITC-dextran dye leak was evaluated as a direct measure of paracellular permeability. Interestingly, only the PC induced FITC-dextran dye leak at 2 h in both normal and high glucose conditions. By 24 h, FITC-dextran dye leak persisted following PC treatment in the high glucose group only. A failure of ZO-1 recovery as well as significantly increased FITC-dextran dye leak in the PC group demonstrated the importance of ensuring this technique is used below its temperature safety threshold. A prolonged loss of ZO-1 localization at the cell membrane as well as loss of cell permeability is associated with loss of RPE functionality, a pathology associated with chronic retinal diseases such as age-related macular degeneration (McLeod, Grebe et al. 2009) and late-stage DR (Simo, Villarroel et al. 2010).

Finally, while it has been established that on a structural level, US-mediated cellular and paracellular permeability is transient, it is also important to ensure that no long-lasting inflammatory stress has been induced following stimulus administration. Consequently, we evaluated NF-κB expression and potential nuclear translocation.

During inflammatory stress, NF-κB translocates from the cell cytoplasm into the nucleus where it acts as a transcription factor to induce expression of several pro-inflammatory cytokines (Barnes and Karin 1997). Our results showed an absence of nuclear translocation of NF-κB in all treatment groups at both 2 and 24 h, indicating that stimulus administration did not trigger any inflammatory response in the cells. More importantly, our study found that US did not induce NF-κB translocation in hyperglycaemic cells, known to be more prone to inflammatory stress. Our findings contradict studies that suggests that US application induces NF-κB nuclear translocation (Hou, Lin et al. 2009, Tang, Liu et al. 2009). Tang et al. (2009) showed that US induced apoptosis of tumour cells therefore induction of NF-κB was a possibility. On the hand, Hou and colleagues (2009) used US at a relatively low intensity of 30 mW/cm^2 but applied it for 20 min, which is 20 times longer than in our study, resulting in induction of inflammation. The differences between our findings and others reflect the adaptability of US with regards to its use and further highlights the need for careful consideration of its intended purpose when determining its optimum dosage.

Although a temperature increase threshold of 1.5 °C has remained the commonly utilised guidance for ocular ultrasound safety, our studies demonstrate that cell stress markers can be increased at temperatures lower than this value. Importantly, LDH release and ZO-1 localisation were affected, especially in the hyperglycaemic state, even below this temperature threshold. While the exact reasons for the heightened susceptibility of cells in high glucose conditions are currently unknown, these findings highlight a need for caution in the use of US for drug delivery in tissues with underlying retinal pathology. In terms of DR, it may be important to either ensure well-controlled glycaemic levels or reduce the applied dose when US therapy is considered within a clinical setting to improve DR therapeutic outcomes. It may also be prudent to look beyond temperature increase alone to better characterise ultrasound safety.

Funding

O.O.M. was supported by an Auckland Medical Research Foundation Grant [1117015].

Data availability statement

The data used in our study are available from the authors upon request.

References

Agban, Y., S. S. Thakur, O. O. Mugisho and I. D. Rupenthal (2019). "Depot formulations to sustain periocular drug delivery to the posterior eye segment." Drug Discovery Today 24(8): 1458-1469.

Barnes, P. J. and M. Karin (1997). "Nuclear factor-kappaB: a pivotal transcription factor in chronic inflammatory diseases." New England Journal of Medicine 336(15): 1066-1071.

Calado, S. M., L. S. Alves, S. Simao and G. A. Silva (2016). "GLUT1 activity contributes to the impairment of PEDF secretion by the RPE." Molecular Vision 22: 761-770.

Cunha-Vaz, J. (2013). The blood-retinal barriers, Springer Science & Business Media.

De Cock, I., E. Zagato, K. Braeckmans, Y. Luan, N. de Jong, S. C. De Smedt and I. J. J. o. c. r. Lentacker (2015). "Ultrasound and microbubble mediated drug delivery: acoustic pressure as determinant for uptake via membrane pores or endocytosis." 197: 20-28.

Domenici, F., C. Giliberti, A. Bedini, R. Palomba, I. Udroiu, L. Di Giambattista, D. Pozzi, S. Morrone, F. Bordi and A. Congiu Castellano (2014). "Structural and permeability sensitivity of cells to low intensity ultrasound: Infrared and fluorescence evidence in vitro." Ultrasonics 54(4): 1020-1028.

Farnoodian, M., C. Halbach, C. Slinger, B. R. Pattnaik, C. M. Sorenson and N. Sheibani (2016). "High glucose promotes the migration of retinal pigment epithelial cells through increased oxidative stress and PEDF expression." American Journal of Physiology: Cell Physiology 311(3): C418-436.

Gemenetzi, M., A. J. Lotery and P. J. Patel (2017). "Risk of geographic atrophy in age-related macular degeneration patients treated with intravitreal anti-VEGF agents." Eye (London, England) 31(1): 1-9.

Geroski, D. H. and H. F. Edelhauser (2000). "Drug delivery for posterior segment eye disease." Investigative Ophthalmology and Visual Science 41(5): 961-964.

Grunwald, J. E., E. Daniel, J. Huang, G. S. Ying, M. G. Maguire, C. A. Toth, G. J. Jaffe, S. L. Fine, B. Blodi, M. L. Klein, A. A. Martin, S. A. Hagstrom, D. F. Martin and C. R. Group (2014). "Risk of geographic atrophy in the comparison of age-related macular degeneration treatments trials." Ophthalmology 121(1): 150-161.

Hou, C. H., J. Lin, S. C. Huang, S. M. Hou and C. H. Tang (2009). "Ultrasound stimulates NF-kappaB activation and iNOS expression via the Ras/Raf/MEK/ERK

signaling pathway in cultured preosteoblasts." Journal of Cellular Physiology 220(1): 196-203.

Huang, D., Y. S. Chen, S. S. Thakur and I. D. Rupenthal (2017). "Ultrasound-mediated nanoparticle delivery across ex vivo bovine retina after intravitreal injection." European Journal of Pharmaceutics and Biopharmaceutics 119: 125-136.

Hughes, P. M., O. Olejnik, J. E. Chang-Lin and C. G. Wilson (2005). "Topical and systemic drug delivery to the posterior segments." Adv Drug Deliv Rev 57(14): 2010-2032.

Kim, Y., M. Prausnitz and H. Edelhauser (2013). "Distribution And Clearance Of Microparticles And Nanoparticles In The Suprachoroidal Space After Injection Using Hollow Microneedles In Rabbits." Investigative Ophthalmology and Visual Science 54(15): 1098-1098.

Kuo, C., C. R. Green, I. D. Rupenthal and O. O. Mugisho (2020). "Connexin43 hemichannel block protects against retinal pigment epithelial cell barrier breakdown." Acta Diabetologica 57(1): 13-22.

Lafond, M., F. Aptel, J. L. Mestas and C. Lafon (2017). "Ultrasound-mediated ocular delivery of therapeutic agents: a review." Expert Opin Drug Deliv 14(4): 539-550.

Lentacker, I., I. De Cock, R. Deckers, S. C. De Smedt and C. T. Moonen (2014). "Understanding ultrasound induced sonoporation: definitions and underlying mechanisms." Adv Drug Deliv Rev 72: 49-64.

Martin, D. F., M. G. Maguire, S. L. Fine, G. S. Ying, G. J. Jaffe, J. E. Grunwald, C. Toth, M. Redford and F. L. Ferris, 3rd (2012). "Ranibizumab and bevacizumab for treatment of neovascular age-related macular degeneration: two-year results." Ophthalmology 119(7): 1388-1398.

McLeod, D. S., R. Grebe, I. Bhutto, C. Merges, T. Baba and G. A. Lutty (2009). "Relationship between RPE and choriocapillaris in age-related macular degeneration." Investigative Ophthalmology and Visual Science 50(10): 4982-4991.

Mugisho, O. O., C. R. Green, D. T. Kho, J. Zhang, E. S. Graham, M. L. Acosta and I. D. Rupenthal (2018). "The inflammasome pathway is amplified and perpetuated in an autocrine manner through connexin43 hemichannel mediated ATP release." Biochim Biophys Acta Gen Subj 1862(3): 385-393.

Mugisho, O. O., C. R. Green, D. Squirrell, S. Bould, J. Zhang, M. Acosta and I. D. Rupenthal (2018). "Intravitreal pro-inflammatory cytokines induce signs of diabetic retinopathy in non-obese diabetic mice." Investigative Ophthalmology and Visual Science 59(9): 5358-5358.

Mugisho, O. O., I. D. Rupenthal, D. M. Squirrell, S. J. Bould, H. V. Danesh-Meyer, J. Zhang, C. R. Green and M. L. Acosta (2018). "Intravitreal pro-inflammatory cytokines

in non-obese diabetic mice: Modelling signs of diabetic retinopathy." PloS One 13(8): e0202156.

Nabili, M., C. Geist and V. Zderic (2015). "Thermal safety of ultrasound-enhanced ocular drug delivery: A modeling study." Medical Physics 42(10): 5604-5615.

Nentwich, M. M. and M. W. Ulbig (2015). "Diabetic retinopathy - ocular complications of diabetes mellitus." World Journal of Diabetes 6(3): 489-499.

Nishijima, K., Y. S. Ng, L. Zhong, J. Bradley, W. Schubert, N. Jo, J. Akita, S. J. Samuelsson, G. S. Robinson, A. P. Adamis and D. T. Shima (2007). "Vascular endothelial growth factor-A is a survival factor for retinal neurons and a critical neuroprotectant during the adaptive response to ischemic injury." American Journal of Pathology 171(1): 53-67.

Paliwal, S. and S. Mitragotri (2006). "Ultrasound-induced cavitation: applications in drug and gene delivery." Expert Opin Drug Deliv 3(6): 713-726.

Park, J., Y. Zhang, N. Vykhodtseva, J. D. Akula and N. J. McDannold (2012). "Targeted and reversible blood-retinal barrier disruption via focused ultrasound and microbubbles." PloS One 7(8): e42754.

Peeters, L., I. Lentacker, R. E. Vandenbroucke, B. Lucas, J. Demeester, N. N. Sanders and S. C. De Smedt (2008). "Can ultrasound solve the transport barrier of the neural retina?" Pharmaceutical Research 25(11): 2657-2665.

Pereira, T. A., D. N. Ramos and R. F. Lopez (2017). "Hydrogel increases localized transport regions and skin permeability during low frequency ultrasound treatment." Scientific Reports 7(1): 44236.

Phenix, C. P., M. Togtema, S. Pichardo, I. Zehbe and L. Curiel (2014). "High intensity focused ultrasound technology, its scope and applications in therapy and drug delivery." Journal of Pharmacy & Pharmaceutical Sciences 17(1): 136-153.

Schlicher, R. K., H. Radhakrishna, T. P. Tolentino, R. P. Apkarian, V. Zarnitsyn and M. R. Prausnitz (2006). "Mechanism of intracellular delivery by acoustic cavitation." Ultrasound in Medicine and Biology 32(6): 915-924.

Shah, R. and V. Zderic (2009). "Ultrasound-enhanced drug delivery through sclera." The Journal of the Acoustical Society of America 125(4): 2680-2680.

Sheikov, N., N. McDannold, S. Sharma and K. Hynynen (2008). "Effect of focused ultrasound applied with an ultrasound contrast agent on the tight junctional integrity of the brain microvascular endothelium." Ultrasound in Medicine and Biology 34(7): 1093-1104.

Simo, R., M. Villarroel, L. Corraliza, C. Hernandez and M. Garcia-Ramirez (2010). "The retinal pigment epithelium: something more than a constituent of the blood-retinal

barrier--implications for the pathogenesis of diabetic retinopathy." Journal of Biomedicine and Biotechnology 2010: 190724.

Sonoda, S., K. Tachibana, T. Yamashita, M. Shirasawa, H. Terasaki, E. Uchino, R. Suzuki, K. Maruyama and T. Sakamoto (2012). "Selective Gene Transfer to the Retina Using Intravitreal Ultrasound Irradiation." Journal of ophthalmology 2012.

Suen, W. L., H. S. Wong, Y. Yu, L. C. Lau, A. C. Lo and Y. Chau (2013). "Ultrasound-mediated transscleral delivery of macromolecules to the posterior segment of rabbit eye in vivo." Investigative Ophthalmology and Visual Science 54(6): 4358-4365.

Tang, W., Q. Liu, X. Wang, P. Wang, J. Zhang and B. Cao (2009). "Potential mechanism in sonodynamic therapy and focused ultrasound induced apoptosis in sarcoma 180 cells in vitro." Ultrasonics 49(8): 786-793.

Thakur, S. S., Y. S. Chen, Z. H. Houston, N. Fletcher, N. L. Barnett, K. J. Thurecht, I. D. Rupenthal and H. S. Parekh (2019). "Ultrasound-responsive nanobubbles for enhanced intravitreal drug migration: An ex vivo evaluation." European Journal of Pharmaceutics and Biopharmaceutics 136: 102-107.

Thakur, S. S., M. S. Ward, A. Popat, N. B. Flemming, M. O. Parat, N. L. Barnett and H. S. Parekh (2017). "Stably engineered nanobubbles and ultrasound - An effective platform for enhanced macromolecular delivery to representative cells of the retina." PloS One 12(5): e0178305.

Thrimawithana, T. R., S. Young, C. R. Bunt, C. Green and R. G. Alany (2011). "Drug delivery to the posterior segment of the eye." Drug Discovery Today 16(5-6): 270-277.

Wei, Y., N. Shang, H. Jin, Y. He, Y. Pan, N. Xiao, J. Wei, S. Xiao, L. Chen and J. Liu (2019). "Penetration of different molecule sizes upon ultrasound combined with microbubbles in a superficial tumour model." Journal of Drug Targeting 27(10): 1068-1075.

Xie, W., S. Liu, H. Su, Z. Wang, Y. Zheng and Y. Fu (2010). "Ultrasound microbubbles enhance recombinant adeno-associated virus vector delivery to retinal ganglion cells in vivo." Academic Radiology 17(10): 1242-1248.

Xu, H. Z., Z. Song, S. Fu, M. Zhu and Y. Z. Le (2011). "RPE barrier breakdown in diabetic retinopathy: seeing is believing." Journal of Ocular Biology, Diseases, and Informatics 4(1-2): 83-92.

Zhang, N., F. Yan, X. Liang, M. Wu, Y. Shen, M. Chen, Y. Xu, G. Zou, P. Jiang, C. Tang, H. Zheng and Z. Dai (2018). "Localized delivery of curcumin into brain with polysorbate 80-modified cerasomes by ultrasound-targeted microbubble destruction for improved Parkinson's disease therapy." Theranostics 8(8): 2264-2277.

Figure Legends

Fig. 1 Plate outline for ultrasound (US) administration. Grey wells contain cells while wells marked '×' represent wells without cells. Experiments were conducted in triplicates. The ultrasound treatments were basal (no US applied), low US (0.2 W/cm^2 and 50% DC), high US (0.5 W/cm^2 and 50% DC), and positive control (PC; 1.0 W/cm^2 and 100% DC)

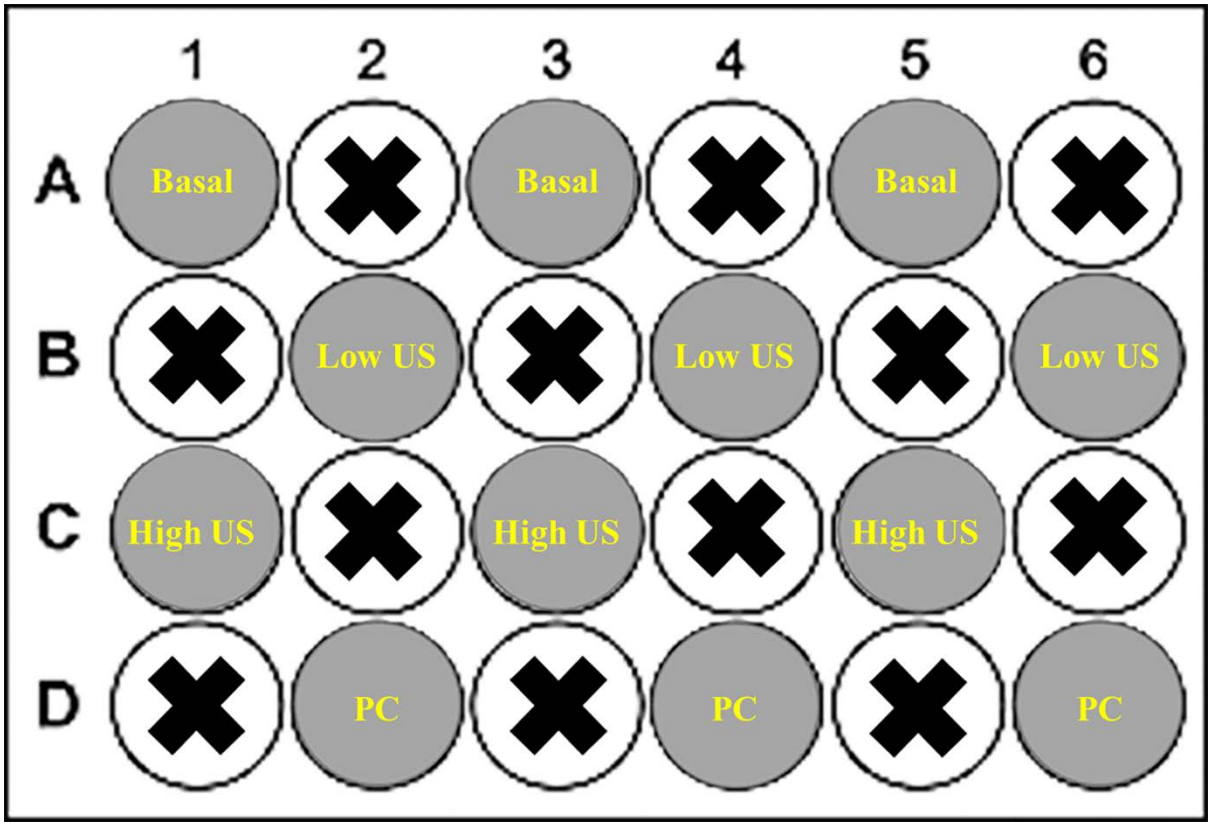

Fig. 2 Thermal effect of different US doses on media temperature. (a-f) Infrared heat map images of media, displaying temperature changes following US exposure. (a) Negative control without US application; (b) 0.2 W/cm^2 intensity with 20% DC, (c) 0.2 W/cm^2 intensity with 50% DC, (d) 0.5 W/cm^2 intensity with 20% DC, (e) 0.5 W/cm^2 intensity with 50% DC US; (f) positive control of 1.0 W/cm^2 intensity with 100% DC US dose. (g) Graph displaying the change in temperature of media without (basal) and with US application. An increase in temperature change was seen with an increase in US intensity and DC. PC US settings resulted in a temperature increase above the 1.5 °C safety threshold as indicated by the dotted red line. Statistical analysis was carried out using one-way ANOVA with Dunnett's multiple comparison's test. n = 3; $^{\#}$denotes statistically significant differences relative to 0.2

W/cm^2 + 20% DC. $^{\#}p \leq 0.05$. *denotes statistically significant differences relative to basal levels. *$p \leq 0.05$; ** $p \leq 0.01$; *** $p \leq 0.001$; **** $p < 0.0001$

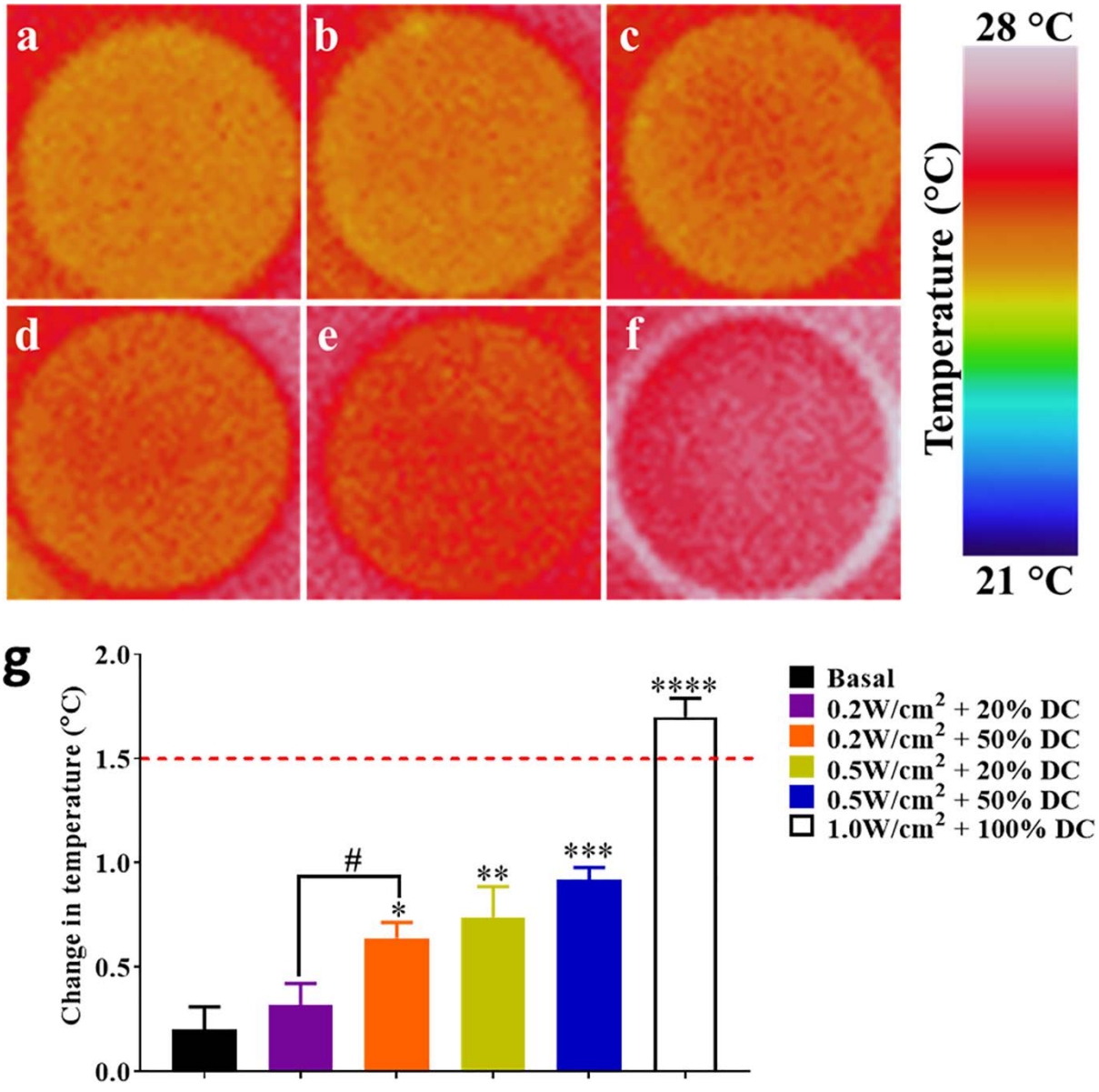

Fig. 3 Effect of glucose levels on ultrasound (US)-mediated LDH release at 30 min (a) and 2 h (b) timepoints. In normal glucose conditions, a significant increase in LDH release was only observed following PC treatment at 30 min. In high glucose conditions, PC treatment induced a significant increase in LDH release at 30 min with high glucose conditions inducing significantly higher LDH release compared to normal glucose conditions across all US treatment groups. By 2 h, a significant increase in LDH release was still observed following high (0.5 W/cm^2 + 50% DC) and PC US treatments comparing high to normal glucose conditions, while even low US treatment still showed elevated LDH release compared to basal. Statistical analysis was carried out using one-way ANOVA with Dunnett's multiple comparison's test. *comparison between normal and high glucose conditions. *p < 0.05; ***p < 0.001; **** p < 0.0001. +comparison between US treatments and basal conditions for either normal or high glucose. +p < 0.05; ++++p < 0.0001. n = 3

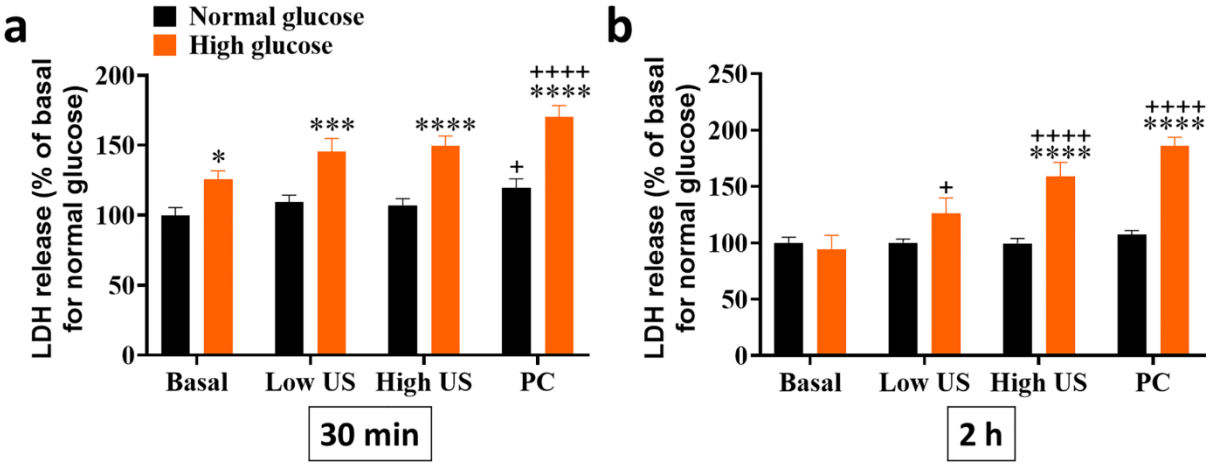

Fig. 4 US treatment did not affect cell morphology or metabolic activity in normal and high glucose conditions. (a) The cell morphology was unchanged in both normal and high glucose conditions across all US treatment groups. (b) US did not induce any changes in metabolic activity in normal glucose conditions. Conversely, high US and PC treatments increased metabolic activity in high glucose conditions. Statistical analysis was carried out using one-way ANOVA with Dunnett's multiple comparison's test. +comparison between US treatments and basal conditions under high glucose. +$p < 0.05$; ++$p < 0.01$. $n = 3$

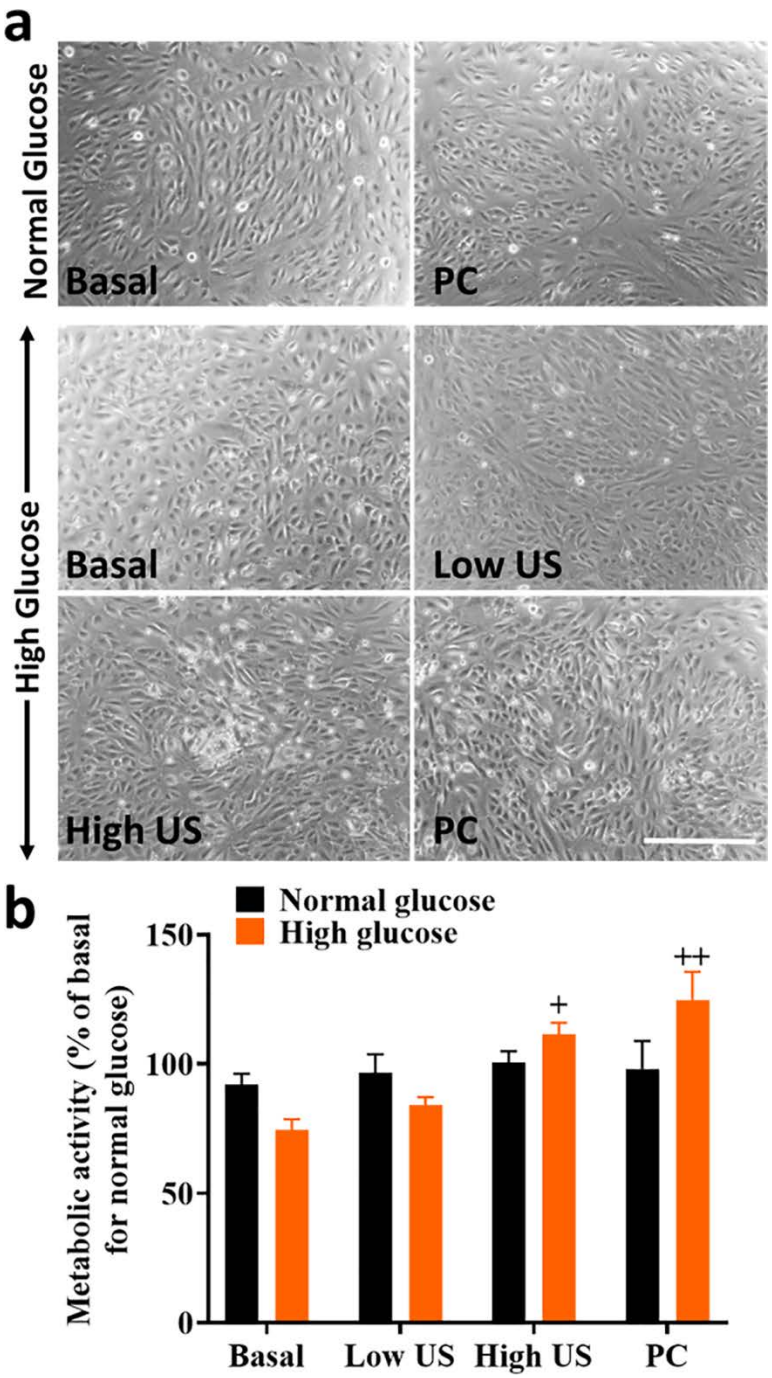

Fig. 5 (a) High glucose treatment exacerbated ultrasound (US)-mediated cell membrane delocalisation of the tight junction protein, ZO-1 (green) at 2 h. In both normal and high glucose groups, ZO-1 localisation at the cell membrane was significantly reduced after application of a low and high US dose (indicated by number of red arrows) compared to basal levels. However, the loss of ZO-1 membrane localisation was more pronounced under high glucose conditions at each US dose. (b) By 24 h, ZO-1 localisation at the cell membrane was restored in both normal and high glucose conditions. However, PC groups showed no recovery of ZO-1 localisation. Cell nuclei stained with DAPI (blue). Scale bar = 50 μm

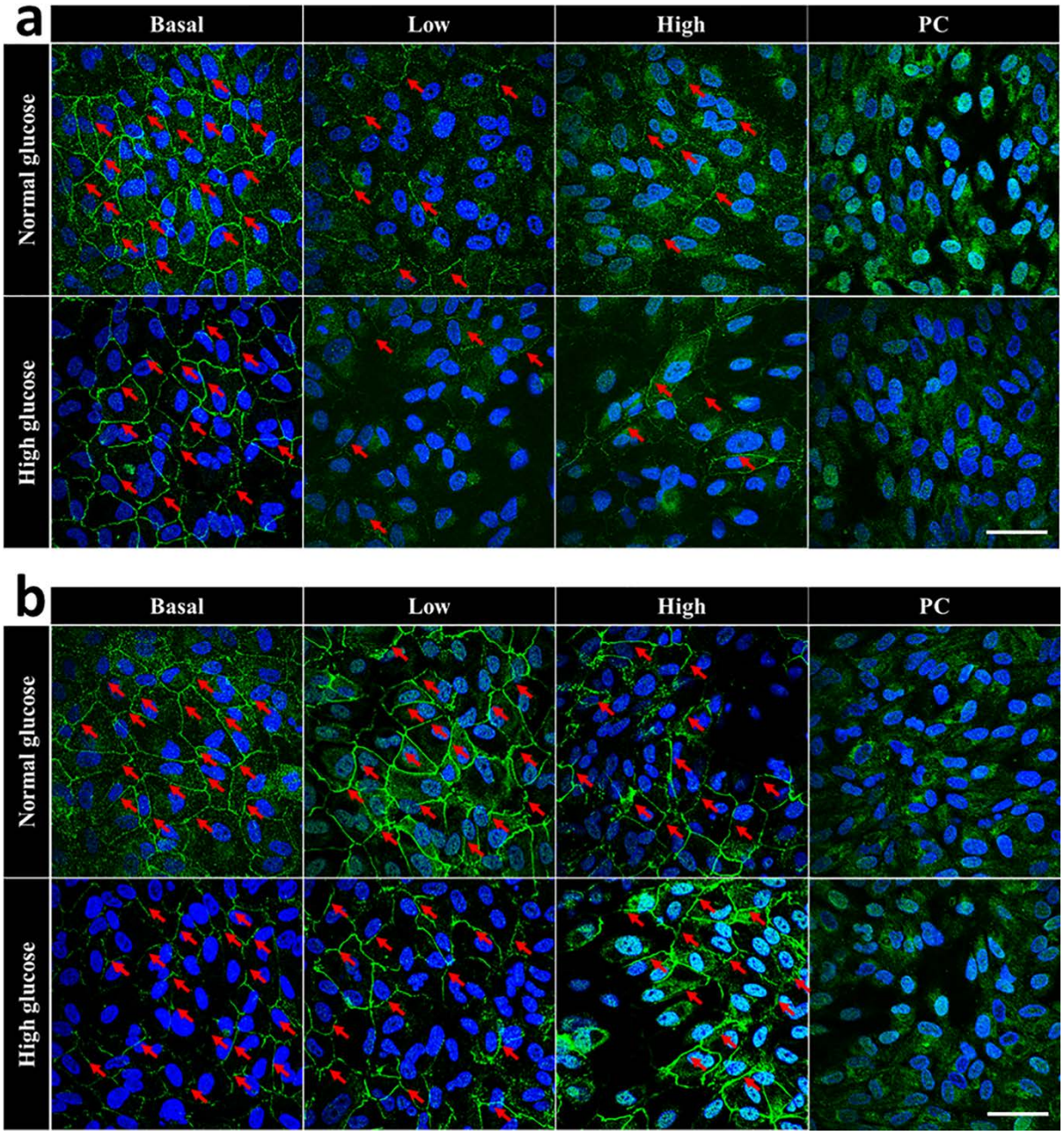

Fig. 6 (a) At 2 h, PC treatment induced FITC-dextran dye leak in both normal and high glucose conditions. (b) By 24 h, FITC-dextran permeability persisted following PC treatment in high but not normal glucose conditions. Statistical analysis was carried out using one-way ANOVA with Dunnett's multiple comparison's test. *comparison between normal and high glucose conditions. **** $p < 0.0001$. +comparison between US treatments and basal conditions. ++++$p < 0.0001$. n = 3

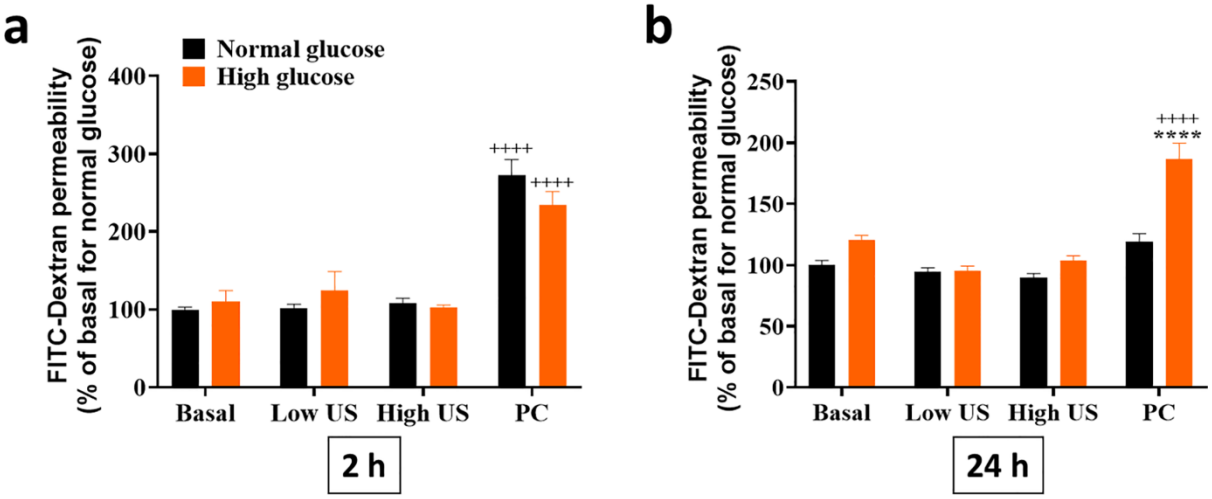

Fig. 7 In both normal and high glucose conditions, US treatment did not induce translocation of NF-κB from the cell cytoplasm to the nucleus. Instead, NF-κB was observed within the cytoplasm alone in all groups studied. Cell nuclei stained with DAPI (blue). Scale bar = 50 μm